GENERATION OF SINGLE ATTOSECOND PULSE BY USING ASYMMETRIC POLARIZATION GATING TECHNOLOGY

H. Liu [1], R. S. Castle [2], A. Y. Z. Feng [1,2*]

[1] School of Chemical and Environmental Engineering, Liaoning University of Technology, Jinzhou 121000, China
[2] Marmara University, Department of Chemical and Environmental Engineering, Istanbul, 34722, Turkey; e-mail: ayzfeng@gmail.com

The generation of high-order harmonics and single attosecond pulses via the asymmetric polarization gating technology has been theoretically investigated. It is shown that when the two circularly polarized laser fields are asymmetric in amplitude and phase, not only can the modulations of the harmonic spectrum be decreased, but also the efficiencies of the harmonics can be enhanced. As a result, a super-continuum with the bandwidth of 85 eV, contributed by the single harmonic emission peak and the near-single short quantum path, can be obtained. Finally, through the Fourier transformation of the selected harmonics on this supercontinuum, a near single attosecond pulse with a full width at half maximum of 52 as can be obtained.

Keywords: *single attosecond pulse, high-order harmonic generation, asymmetric polarization gating technology.*

ГЕНЕРАЦИЯ ОДИНОЧНОГО АТТОСЕКУНДНОГО ИМПУЛЬСА С ИСПОЛЬЗОВАНИЕМ МЕТОДА АСИММЕТРИЧНОГО ПОЛЯРИЗАЦИОННОГО СТРОБИРОВАНИЯ

H. Liu [1], R. S. Castle [2], A. Y. Z. Feng [1,2*]

УДК 538.551.3

[1] Школа химической и экологической инженерии, Ляонинский технологический университет, Цзиньчжоу 121000, Китай
[2] Университет Мармара, Стамбул, 34722, Турция; e-mail: ayzfeng@gmail.com

(Поступила 9 апреля 2018)

Теоретически исследована генерация гармоник высокого порядка и одиночных аттосекундных импульсов с помощью метода асимметричного поляризационного стробирования. Показано, что при амплитудной и фазовой асимметрии двух циркулярно поляризованных лазерных полей можно не только уменьшить модуляции гармонического спектра, но и повысить эффективность гармоник. В результате может быть получен суперконтинуум с шириной полосы 85 эВ, обусловленный пиком излучения одиночной гармоники и практически одним коротким квантовым путем. Посредством преобразования Фурье избранных гармоник на суперконтинууме можно получить почти одиночный аттосекундный импульс с полной шириной на половине максимума 52 ас.

Ключевые слова: *одиночный аттосекундный импульс, генерация гармоник высокого порядка, метод асимметричного поляризационного стробирования.*

Introduction. High-order harmonic generation (HHG) has attracted lots of attention in the past two decades because the emitted radiation emerges as a broad spectrum with attosecond temporal structure, which may serve as an important tool for accessing the ultrafast scales relevant to the electron dynamics in atoms, molecules, solids and materials etc. [1–8]. Currently, the physical mechanism of HHG can be well explained through the semiclassical three-step model (STM) [9] with the processes of ionization, acceleration, and recombination. Finally, harmonics with maximum energy up to $I_p + 3.17(I/4\omega^2)$ can be obtained, where I_P, I, and ω are the first ionization potential, the laser intensity, and the laser frequency, respectively.

On the basis of the STM, the HHG emits coherent bursts of light in each optical half-cycle of the laser field, which leads to the generations of the attosecond pulse trains with two main bursts in one optical cycle. However, the single attosecond pulses (SAPs) are much more favorable to explore the ultrafast electronic dynamics. Thus, two techniques have been used out to obtain SAPs with the higher photon energy. Particularly, (i) the first and the simplest method to obtain the SAPs is to reduce the harmonic emission path by using the shorter pulse duration. For instance, by using the single-cycle 3.3 fs pulse, Goulielmakis et al. [10] obtained a SAP with full width at half maximum (FWHM) of 80 as. However, the production of the carrier-envelope phase (CEP) stable few-cycle pulse is still a challenge in many laboratories; thus, the universality of the above scheme is decreased. To overcome this weakness, many improved methods have been proposed, such as the two-color or the three-color synthesized field scheme [11–14] and the frequency modulation scheme by using the chirped pulse [15–17], etc. (ii) On the other hand, the HHG from the polarization gating (PG) field [18–20], consisting of corotating and counterrotating circularly polarized laser fields with a different delay time, is another effective method to produce the SAPs. For instance, by using the PG technique, Sansone et al. [21] obtained a 130 as SAP. Li et al. [22] obtained the SAPs in the water window by using the mid-infrared PG field. However, the most important drawback of the PG scheme is the low conversion efficiency of the produced HHG. Therefore, to obtain the high-intensity SAPs, an improved PG scheme, namely double optical gating (DOG), has been proposed. For instance, Mashiko et al. [23] experimentally obtained an isolated 130 as pulse by using the phase stabilized DOG scheme. Zhao et al. [24] experimentally obtained a single 67 as pulse, which is the shortest SAP so far. Feng et al. [25] theoretically predicted a 33 as pulse by using the inhomogeneous DOG scheme.

In this paper, an effective scheme to enhance the intensities of the SAPs has been proposed via the asymmetric PG technology. It is found that by properly choosing the amplitude and phase of the two circularly polarized pulses, not only can the single short quantum path be selected to contribute to the HHG, but also the harmonic yield can be enhanced, showing a supercontinuum with the bandwidth of 85 eV. Finally, by directly superposing this supercontinuum, a near-SAP with the FWHM of 52 as can be produced. Atomic units (a.u.) are used throughout this paper unless stated otherwise.

Calculations. The HHG from H_2^+ can be investigated by solving the two-dimensional time-dependent Schrödinger equation (2D-TDSE) [26–30]

$$i\partial\psi(x, y, z)/\partial t = [(-1/2)\partial^2/\partial x^2 - (1/2)\partial^2/\partial y^2 + V(x, y) + xE_x(x, t) + yE_y(y, t)]\psi(x, y, z), \quad (1)$$

where $V(x,y) = -1.0/\sqrt{(x+R/2)^2 + y^2 + 0.5} - 1.0/\sqrt{(x-R/2)^2 + y^2 + 0.5}$ is the soft Coulomb potential for H_2^+ ion, x and y are the electronic coordinates, and $R = 2.0$ a.u. is the internuclear distance of H_2^+ ion.

The synthesized PG laser field consists of the corotating and the counterrotating circularly polarized laser fields with different delay time

$$E_x(t) = E_1 f(t - t_{\text{delay}}/2)\cos(\omega_1 t + \varphi_1) + E_2 f(t + t_{\text{delay}}/2)\cos(\omega_2 t + \varphi_2), \quad (2)$$

$$E_y(t) = E_1 f(t - t_{\text{delay}}/2)\sin(\omega_1 t + \varphi_1) - E_2 f(t + t_{\text{delay}}/2)\sin(\omega_2 t + \varphi_2), \quad (3)$$

$$f(t) = \exp[-4\ln(2)t^2/\tau_i^2]. \quad (4)$$

Here, E_i, ω_i, τ_i, and φ_i ($i = 1, 2$) are the amplitudes, frequencies, pulse duration, and the CEPs of the two circularly polarized pulses, and t_{delay} is the delay time between the two pulses.

The HHG spectra are given by

$$S(\omega) = \left|\left(1/\sqrt{2\pi}\right)\int d_A(t)e^{-i\omega t}dt\right|^2, \quad (5)$$

where $d_A(t) = -\left\langle \psi(x,y,t) \middle| \begin{matrix} \partial V(x,y)/\partial x + E_x(t) \\ +\partial V(x,y)/\partial y + E_y(t) \end{matrix} \middle| \psi(x,y,t) \right\rangle$.

Finally, the signal of the SAP can be given by

$$I_{\text{SAP}}(t) = |\textstyle\sum_q[\int d_A(t)e^{-iq\omega t}]e^{iq\omega t}|^2. \quad (6)$$

Results and discussion. Figure 1 shows the HHG spectra driven by the symmetric PG laser field. The laser parameters of the corotating and counterrotating circularly polarized laser fields are chosen to be $I_{1,2} = 3.0\times10^{14}$ W/cm^2, $\lambda_{1,2} = 800$ nm, $\tau_{1,2} = 10$ fs, and $\varphi_{1,2} = 0.0\pi$. For the case of $t_{\text{delay}} = 0.0$ fs (corresponding to the linearly polarized laser field on the x axis), the typical characteristic on the HHG spectrum can be obtained, that is, the intensities of the harmonics can be rapidly decreased during the first few orders; then

a harmonic plateau with the stable intensity can be found; finally, a harmonic cutoff with the value of $165\omega_1$ can be produced. As can be seen, although the harmonic cutoff driven by the linearly polarized combined field (t_{delay} = 0.0 fs) can be extended to the $165\omega_1$, the larger modulations on the HHG spectrum are not beneficial for producing the SAPs. As t_{delay} increases, the modulations of the harmonics can be decreased, but they are still too large to support the SAPs. Moreover, with increase in the delay time, the efficiency of HHG is also decreased, which is unfavorable to improve the intensities of the attosecond pulses.

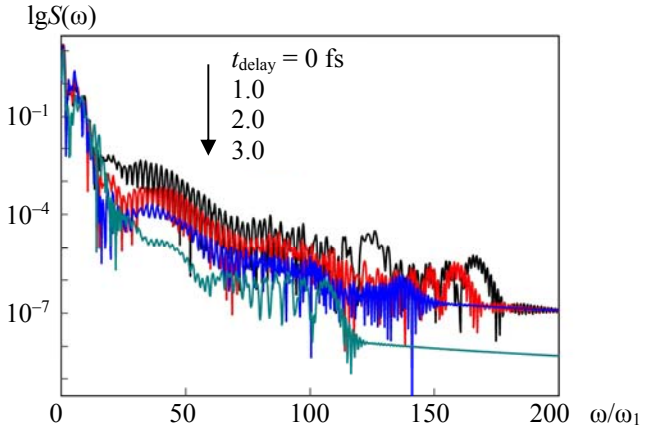

Fig. 1. The HHG spectra driven by the symmetric PG laser field. The laser parameters of the corotating and the counterrotating circular polarization laser fields are chosen to be $I_{1,2} = 3.0\times10^{14}$ W/cm^2, $\lambda_{1,2}$ = 800 nm, $\tau_{1,2}$ = 10 fs, and $\varphi_{1,2} = 0.0\pi$.

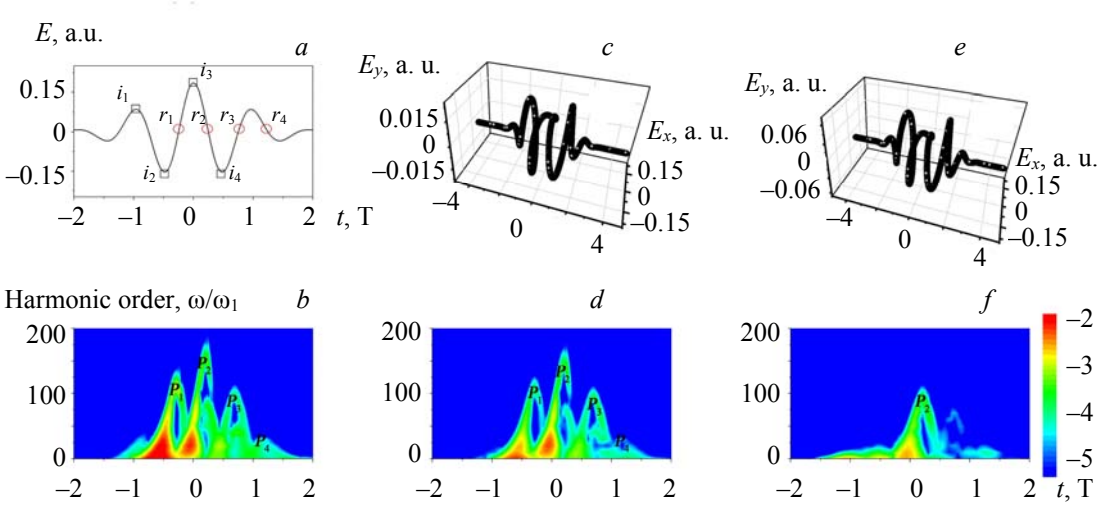

Fig. 2. The laser profiles of the symmetric PG laser field with t_{delay} = 0 (a), 1.0 (c), and 3.0 fs (e). The time-frequency analyses of the HHG for the cases of the symmetric PG laser fields with t_{delay} = 0 (b), 1.0 (d), and 3.0 fs (f). T indicates the optical cycle of 800 nm pulse in all the following figures unless stated otherwise.

Figure 2 shows the laser profiles and the time-frequency analyses of the HHG [31] for the cases of the above symmetric PG laser fields with t_{delay} = 0, 1.0, and 3.0 fs, respectively. For the case of t_{delay} = 0.0 fs, based on the STM, there are four main ionization times during the present laser driven time, marked as $i_{1–4}$ (Fig. 2a). Then, after the next half cycles, the accelerated electron can recombine with its parent ions around $r_{1\sim4}$ points. As a result, four harmonic emission peaks (HEPs) can be obtained during the harmonic emission process, marked as $P_{1–4}$ (Fig. 2b). As can be seen, when the harmonics are higher than the $20\omega_1$, the signals of the HHG spectrum are contributed by $P_{1\sim3}$. Moreover, the contributions of each HEP comes from the coupling of the short and the long quantum paths, which is responsible for the larger modulations on the HHG

spectrum. For the case of t_{delay} = 1.0 fs, the polarization of the combined circularly polarized laser field can be changed (Fig. 2c). As a result, the contribution of the long quantum path can be decreased on the HHG spectrum in comparison with that from t_{delay} = 0.0 fs case, which leads to the decrease of the modulations on the HHG spectrum (Fig. 2d). Moreover, the intensities of the HEPs from the rising and the falling parts of the laser field are also decreased compared with those from t_{delay} = 0.0 fs case, which is responsible for the intensity decrease of the harmonic yield. As t_{delay} further increases (Fig. 2e), the signal of the HHG spectrum is only contributed by P_2, which is responsible for the intensity decrease and the modulation suppression of the HHG spectrum (Fig. 2f). Here, although the signal of the HHG spectrum is only coming from one HEP for t_{delay} = 3.0 fs, the larger coupling of the two quantum paths is still not beneficial for generating the SAPs.

Figure 3 shows the HHG spectra driven by the asymmetric PG laser field. The laser parameters of the corotating and the counterrotating circularly polarized laser fields are chosen to be $I_{1,2} = 3.0\times10^{14}$ W/cm^2, $\lambda_{1,2}$ = 800 nm, $\tau_{1,2}$ = 10 fs, $\varphi_1 = 1.0\pi$, and $\varphi_2 = 0.0\pi$ (asymmetric PG technology in CEPs). For the case of t_{delay} = 0.0 fs (corresponding to the linearly polarized laser field on the y axis), the modulations of the harmonics are decreased compared with those from the symmetric PG technology with t_{delay} = 0.0 fs. Moreover, a smooth harmonic plateau from the $85\omega_1$ to the $155\omega_1$ can be obtained. For the case of t_{delay} = 1.0 fs, although the efficiency of HHG is slightly decreased, a much smoother harmonic plateau from the $20\omega_1$ to the $145\omega_1$ can be produced. As t_{delay} further increases (i.e., t_{delay} = 2.0 fs), the harmonic cutoff and the harmonic yield are both decreased, which is not good for generating the high-intensity SAPs.

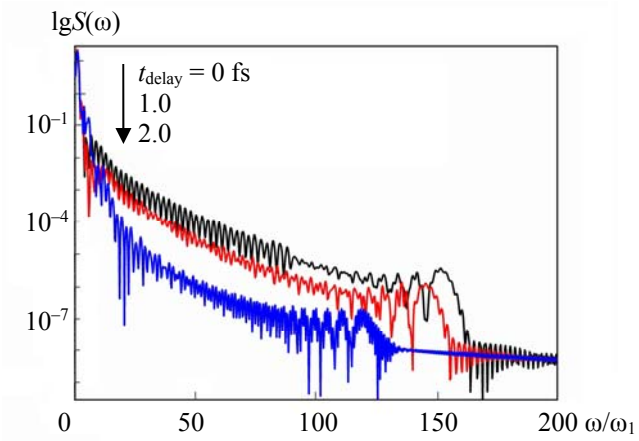

Fig. 3. The HHG spectra driven by the asymmetric PG laser field. The laser parameters of the corotating and the counterrotating circularly polarized laser fields are chosen to be $I_{1,2} = 3.0\times10^{14}$ W/cm^2, $\lambda_{1,2}$ = 800 nm, $\tau_{1,2}$ = 10 fs, $\varphi_1 = 1.0\pi$, and $\varphi_2 = 0\pi$ (asymmetric PG technology in CEPs).

Figure 4 shows the laser profiles and the time-frequency analyses of the HHG for the cases of the above asymmetric PG laser fields with t_{delay} = 0, 1.0, and 2.0 fs, respectively. For the case of t_{delay} = 0 fs, the four HEPs can also be found during the harmonic emission process (Figs. 4a,b). However, the intensity of P_3 is very weak in comparison with those of P_1 and P_2. This means the contributions of the HHG spectrum are mainly coming from P_1 and P_2, which is the reason behind the decreased modulations on the HHG spectrum. Moreover, when the harmonics are higher than the $85\omega_1$, the contribution of the HHG spectrum is mainly from P_2, and the intensity of the short quantum path is higher than that of the long quantum path, which leads to the smooth harmonic plateau in this region. For the case of t_{delay} = 1.0 fs (Figs. 4c,d), the intensities of P_1 and P_2 are decreased, but the intensity of P_3 is slightly enhanced. Moreover, the intensities of the long quantum paths for these three HEPs are all reduced. As a result, when the harmonics are higher than the $20\omega_1$, although the signals of the HHG spectrum are contributed by P_{1-3}, the contribution of P_2 plays the main role in the HHG spectrum, which is the reason behind the smoother harmonic plateau from the $20\omega_1$ to the $145\omega_1$. For the case of t_{delay} = 2.0 fs (Figs. 4e,f), the signal of the HHG spectrum comes mainly from P_3, and its intensity is very weak compared with that of P_2 in Figs. 4b,d. Therefore, the intensity of the HHG spectrum from t_{delay} = 2.0 fs will be decreased compared with those from the smaller delay times. It should be noted that although the signal of the HHG spectrum is only contributed by P_3, the comparable coupling of the two quantum paths are still not beneficial for generating the SAPs.

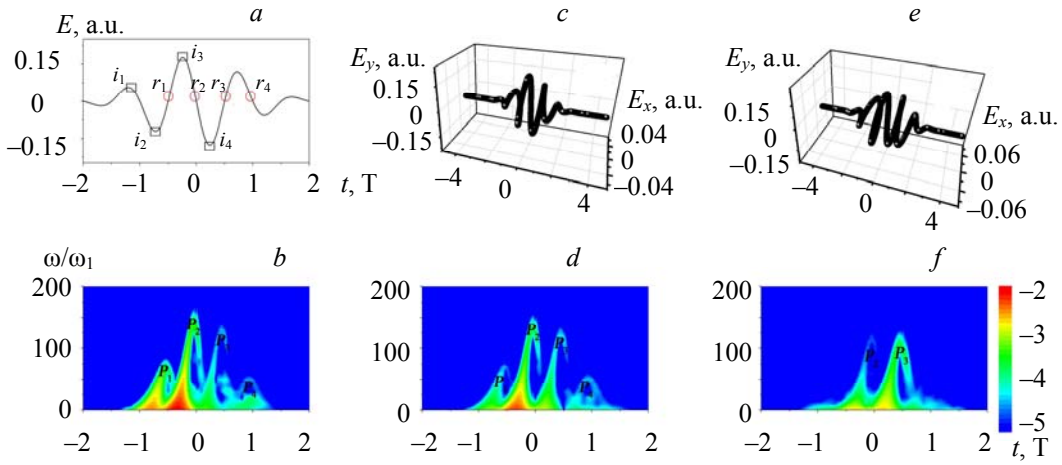

Fig. 4. The laser profiles of the CEP asymmetric PG laser field with t_{delay} = 0 (a), 1.0 (c), and 2.0 fs (e). The time-frequency analyses of the HHG for the cases of the CEP asymmetric PG laser fields with t_{delay} = 0.(b), 1.0 (d), and 2.0 fs (f).

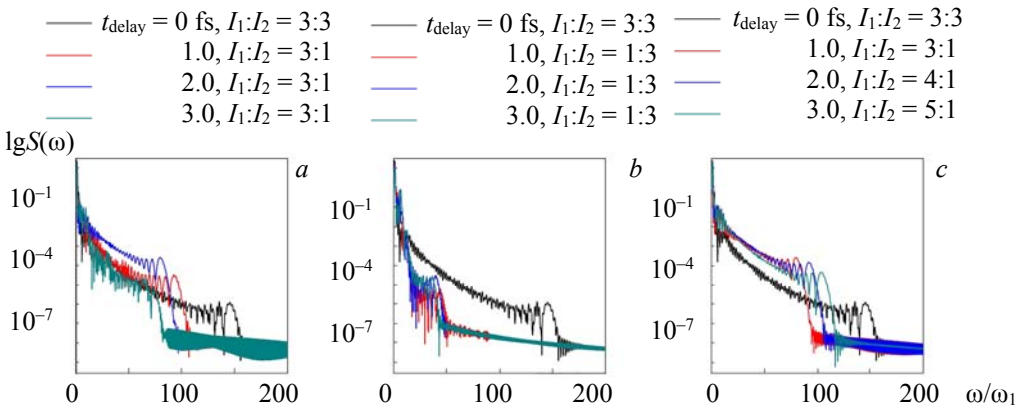

Fig. 5. The HHG spectra for the cases of the asymmetric PG technology in laser intensity. The laser intensities are chosen to be (a) $I_1 = 3.0\times10^{14}$ W/cm^2, $I_2 = 1.0\times10^{14}$ W/cm^2 (marked as I_1:I_2 = 3:1), (b) $I_1 = 1.0\times10^{14}$ W/cm^2, $I_2 = 3.0\times10^{14}$ W/cm^2 (I_1:I_2 = 1:3), (c) $I_1 = 4.0\times10^{14}$ W/cm^2, $I_2 = 1.0\times10^{14}$ W/cm^2 and $I_1 = 5.0\times10^{14}$ W/cm^2, $I_2 = 1.0\times10^{14}$ W/cm^2 (I_1:I_2 = 4:1 and I_1:I_2 = 5:1). The CEPs of the two pulses are $\varphi_1 = 1.0\pi$ and $\varphi_2 = 0.0\pi$.

Figures 5a,b show the HHG spectra for the cases of the asymmetric PG technology in laser intensity. The laser intensities are chosen to be (i) $I_1 = 3.0\times10^{14}$ W/cm^2, and $I_2 = 1.0\times10^{14}$ W/cm^2 for Fig. 5a (marked as I_1:I_2 = 3:1) and (ii) $I_1 = 1.0\times10^{14}$ W/cm^2, and $I_2 = 3.0\times10^{14}$ W/cm^2 for Fig. 5b (I_1:I_2 = 1:3). The other laser parameters are chosen to be $\lambda_{1,2}$ = 800 nm, $\tau_{1,2}$ = 10 fs, $\varphi_1 = 1.0\pi$, and $\varphi_2 = 0.0\pi$. For comparison, the HHG spectrum driven by the asymmetric PG laser field with I_1:I_2 = 3:3 and t_{delay} = 1.0 fs is also shown. Clearly, for the cases of I_1:I_2 = 3:1 (Fig. 5a), the harmonic cutoff will be decreased as t_{delay} increases; however, the modulations of the harmonics can also be decreased, and the efficiency of HHG can be enhanced. Especially for the case of t_{delay} = 2.0 fs, an intense and smooth harmonic plateau from the $20\omega_1$ to the $80\omega_1$ can be obtained. For the cases of I_1:I_2 = 1:3 (Fig. 5b), the efficiency of HHG is decreased, and the modulations on the HHG spectrum are enhanced, which is not beneficial for the generation of the high-intensity SAPs. Figure 5c shows the HHG spectra for the cases of I_1:I_2 = 4:1 and I_1:I_2 = 5:1 with t_{delay} = 2.0 fs. Clearly, as the intensity of the co-rotating circularly polarized laser field further increases, the harmonic cutoff can be extended, but the efficiency of HHG is slightly decreased.

Figure 6 shows the laser profiles and the time-frequency analyses of the HHG for the cases of the above asymmetric PG laser fields with I_1:I_2 = 3:1, t_{delay} = 2.0 fs and I_1:I_2 = 1:3, t_{delay} = 2.0 fs, respectively. For the case of I_1:I_2 = 3:1 and t_{delay} = 2.0 fs (Figs. 6a,b), when the harmonics are higher than the $20\omega_1$, the contribution of the HHG spectrum is only coming from P_2. Moreover, the intensity of the short quantum path from P_2 is much higher than that of the long quantum path from P_2, which is the reason behind the smaller modulations on the HHG spectrum and is favorable to produce the SAPs. Furthermore, the intensity of P_2 is much higher than that from the I_1:I_2 = 3:3 and t_{delay} = 1.0 fs case (compared with Fig. 4d,b), which leads to the intensity enhancement of the harmonic yield. For the case of I_1:I_2 = 1:3 and t_{delay} = 2.0 fs (Figs. 6c,d), the contribution of the HHG spectrum is mainly from P_4 with the smaller photon energy and the lower intensity. Moreover, the larger coupling of the two quantum paths from P_4 can also be found. These are the reasons behind the lower harmonic yield with the larger modulations on the HHG spectrum.

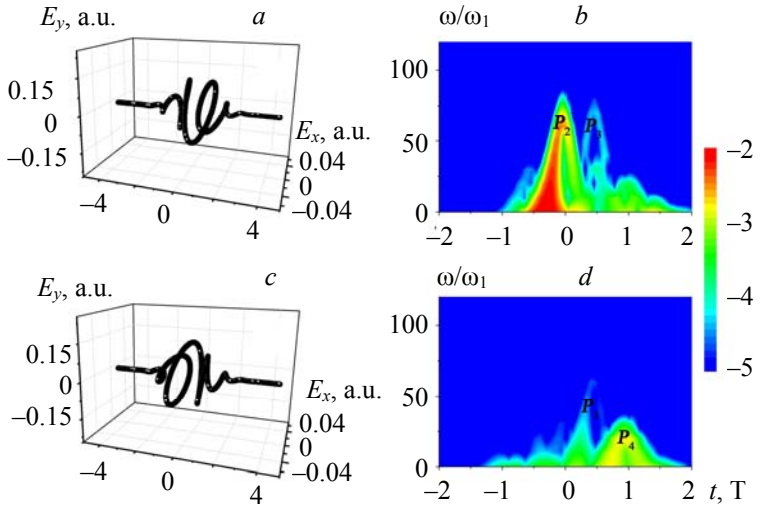

Fig. 6. The laser profiles and the time-frequency analyses of the HHG for the cases of the above asymmetric PG laser fields with (a) and (b) I_1:I_2 = 3:1, t_{delay} = 2.0 fs; (c) and (d) I_1:I_2 = 1:3, t_{delay} = 2.0 fs.

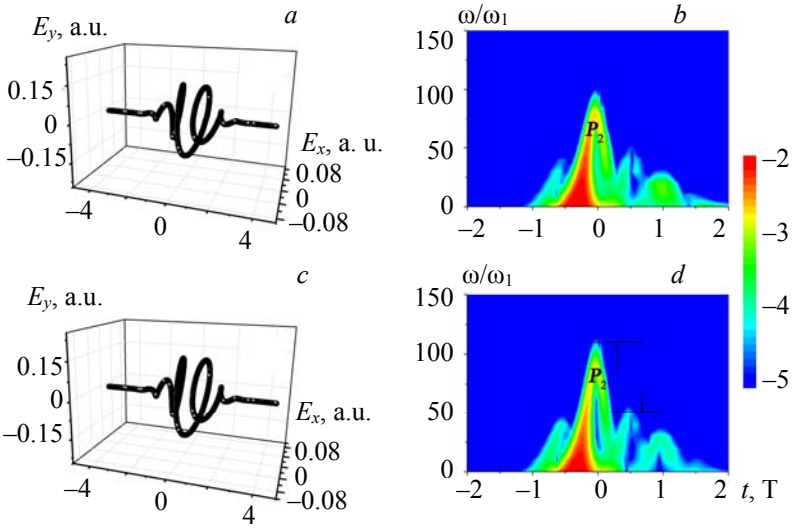

Fig. 7. The laser profiles and the time-frequency analyses of the HHG for the cases of the above asymmetric PG laser fields with I_1:I_2 = 4:1, t_{delay} = 2.0 fs (a, b); I_1:I_2 = 5:1, t_{delay} = 2.0 fs (c, d).

Figure 7 shows the laser profiles and the time-frequency analyses of the HHG for the cases of the above asymmetric PG laser fields with I_1:I_2 = 4:1, t_{delay} = 2.0 fs and I_1:I_2 = 5:1, t_{delay} = 2.0 fs, respectively. As can be seen, with the intensity enhancement of the co-rotating circularly polarized laser field, the HEP of P_2 is extended, which is responsible for the cutoff extension on the HHG spectrum shown in Fig. 5c. Furthermore, for the case of I_1:I_2 = 5:1 and t_{delay} = 2.0 fs (Figs. 7c,d), when the harmonics are higher than the $50\omega_1$, the signal of the HHG spectrum is only contributed by P_2. Moreover, the intensity of the short quantum path from P_2 is higher than that of the long quantum path from P_2, thus leading to a supercontinuum with the smaller harmonic modulations and is much better for producing the SAPs.

As discussed before, the modulations of the harmonics, caused by the coupling of the two quantum paths, play an important role in producing the SAPs. In this paper, we see that by using the asymmetric PG technology, the signal of the harmonic plateau only comes from one HEP with the dominant short quantum path contribution. As a consequence, a supercontinuum with the bandwidth of 85 eV can be obtained. Now, by directly superposing this supercontinuum (generated from the asymmetric PG laser field with $\varphi_1 = 1.0\pi$, $\varphi_2 = 0.0\pi$, I_1:I_2 = 5:1 and t_{delay} = 2.0 fs), a near-single attosecond pulse with the FWHM of 52 as can be produced, as shown in Fig. 8a. To show the advantage for using the asymmetric PG technology to produce the SAPs, the temporal profiles of the attosecond pulses produced from the symmetric PG technology with $\varphi_1 = \varphi_2 = 0.0\pi$, I_1:I_2 = 3:3, and t_{delay} = 0.0 fs are shown in Figs. 8b,c. As can be seen, by superposing the harmonics (generated from the symmetric PG laser field) from the $65\omega_1$ to the $165\omega_1$ or from the $135\omega_1$ to the $165\omega_1$, due to the multi-HEPs during the harmonic emission process, the attosecond pulse trains with the multi-peaks in one optical cycle can be obtained, which is not beneficial in practical applications.

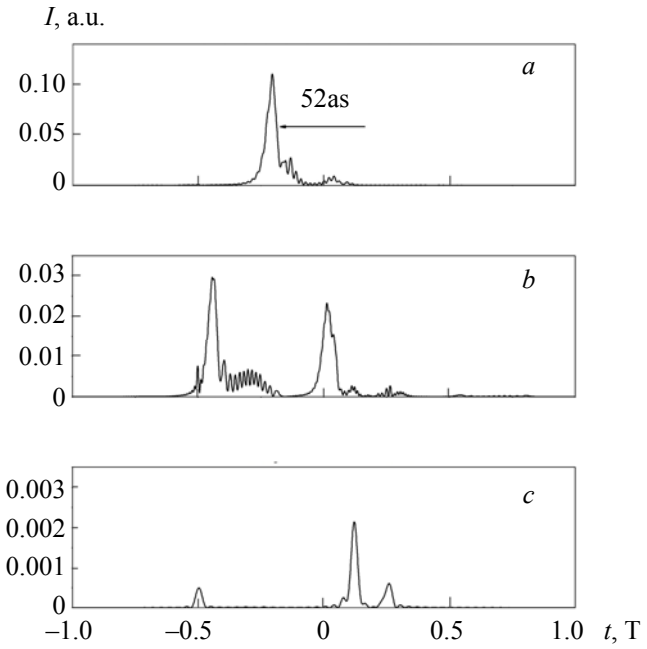

Fig. 8. The temporal profiles of the attosecond pulse by superposing the harmonics of the (a) asymmetric PG laser field with I_1:I_2 = 5:1 and t_{delay} = 2.0 fs from the $50\omega_1$ to the $105\omega_1$ and (b, c) symmetric PG laser field with I_1:I_2 = 3:3 and t_{delay} = 0.0 fs (b) from the $65\omega_1$ to the $165\omega_1$ and (c) from the $135\omega_1$ to the $165\omega_1$; (a) $\varphi_1 = 1.0\pi$, $\varphi_2 = 0$; (b, c) $\varphi_1 = \varphi_2 = 0$

Conclusion. We theoretically investigated the asymmetric PG effect on the generations of the HHG and the SAPs. The results show that by properly changing the amplitudes and the phases of the corotating and the counterrotating circularly polarized laser fields in asymmetry, not only can the intensities of the harmonics be enhanced, but also the harmonic emission process can be selected and controlled. Consequently, a supercontinuum with the bandwidth of 85 eV, contributed by single HEP with the short quantum path, can be obtained. Further, by directly superposing the harmonics from this supercontinuum, a near-SAP with the FWHM of 52 as can be obtained.

Acknowledgment. This work was supported by National Natural Science Foundation of China (No. 11504151) and the Doctoral Scientific Research Foundation of Liaoning Province, China (No. 201501123).

REFERENCES

1. F. Krausz, M. Ivanov, *Rev. Mod. Phys.*, **81**, 163–234 (2009).
2. G. Vampa, T. J. Hammond, N. Thiré, B. E. Schmidt, F. Légaré, C. R. McDonald, T. Brabec, P. B. Corkum, *Nature*, **462**, 522–526 (2015).
3. T. T. Luu, M. Garg, S. Y. Kruchinin, A. Moulet, M. T. Hassan, E. Goulielmakis, *Nature*, **521**, 498–502 (2015).
4. P. C. Li, C. Laughlin, S. I. Chu, *Phys. Rev. A*, **89**, 023431 (2014).
5. K. J. Yuan, A. D. Bandrauk, *Phys. Rev. Lett.*, **110**, 023003 (2013).
6. X. B. Bian, A. D. Bandrauk, *Phys. Rev. Lett.*, **105**, 093903 (2010).
7. M. F. Ciappina, J. A. Pérez-Hernández, A. S. Landsman, W. Okell, S. Zherebtsov, B. Förg, J. Schötz, J. L. Seiffert, T. Fennel, T. Shaaran, T. Zimmermann, A. Chacón, R. Guichard, A. Zaïr, J. W. G. Tisch, J. P. Marangos, T. Witting, A. Braun, S. A. Maier, L. Roso, M. Krüger, P. Hommelhoff, M. F. Kling, F Krausz, M Lewenstein, *Rep. Prog. Phys*., **80**, 054401 (2017).
8. R. E. F. Silva, F. Catoire, P. Riviere, H. Bachau, F. Martin, *Phys. Rev. Lett.*, **110**, 113001 (2013).
9. P. B. Corkum, *Phys. Rev. Lett.*, **71**, 1994–1997 (1993).
10.E. Goulielmakis, M. Schultze, M. Hofstetter, V. S. Yakovlev, J. Gagnon, M. Uiberacker, A. L. Aquila, E. M. Gullikson, D. T. Attwood, R. Kienberger, F. Krausz, U. Kleineberg, *Science*, **320**, 1614–1617 (2008).
11. Z. Zeng, Y. Cheng, X. Song, R. Li, Z. Xu, *Phys. Rev. Lett.*, **98**, 203901 (2007).
12. C. L. Xia, X. S. Liu, *Phys. Rev. A*, **87**, 043406 (2013).
13. X. Wang, C. Jin, C. D. Lin, *Phys. Rev. A*, **90**, 023416 (2014).
14. T. Popmintchev, M. C. Chen, O. Cohen, M. Grisham, J. Rocca, M. Murnane, H. Kapteyn, *Opt. Lett.*, **33**, 2128–2130 (2008).
15. J. J. Xu, B. Zeng, Y. L. Yu, *Phys. Rev. A*, **82**, 053822 (2010).
16. L. Q. Feng, T. S. Chu, *Phys. Rev. A*, **84**, 053853 (2011).
17. L. Q. Feng, *Phys. Rev. A*, **92**, 053832 (2015).
18. P. B. Corkum, N. H. Burnett, M. Y. Ivanov, *Opt. Lett.*, **19**, 1870–1872 (1994).
19. Z. Chang, *Phys. Rev. A*, **71**, 023813 (2005).
20. F. Ferrari, F.Calegari, M. Lucchini, C. Vozzi, S. Stagira, G. Sansone, M. Nisoli, *Nat. Photonics*, **4**, 875–879 (2010).
21. G. Sansone, E. Benedetti, F. Calegari, C. Vozzi, L. Avaldi, R. Flammini, L. Poletto, P. Villoresi, C. Altucci, R. Velotta, S. Stagira, S. De Silvestri, M. Nisoli, *Science*, **314**, 443–446 (2006).
22. J. Li, X. M. Ren, Y. C. Yin, Y. Cheng, E. Cunningham, Y. Wu, Z. H. Chang, *Appl. Phys. Lett.*, **108**, 231102 (2016).
23. H. Mashiko, S. Gibertson, C. Q. Li, S. D. Khan, M. M. Shakya, E. Moon, Z. H. Chang, *Phys. Rev. Lett.*, **100**, 103906 (2008).
24. K. Zhao, Q. Zhang, M. Chini, Y. Wu, X. W. Wang, Z. H. Chang, *Opt. Lett.*, **37**, 3891–3893 (2012).
25. L. Q. Feng, W. L. Li, R. S. Castle, *J. Appl. Spectrosc.*, **85**, 171 (2018).
26. R. F. Lu, P. Y. Zhang, K. L. Han, *Phys. Rev. E*, **77**, 066701 (2008).
27. J. Hu, K. L. Han, G. Z. He, *Phys. Rev. Lett.*, **95**, 123001 (2005).
28. L. Q. Feng, H. Liu, *Phys. Plasmas*, **22**, 013107 (2015).
29. L. Q. Feng, W. L. Li, H. Liu, *Ann. Phys.* (*Berlin*), **529**, 1700093 (2017).
30. X. Cao, S. C. Jiang, C. Yu, Y. H. Wang, L. H. Bai, R. F. Lu, *Opt. Express*, **22**, 26153–26161 (2014).
31. P. Antoine, B. Piraux, A. Maquet, *Phys. Rev. A*, **51**, R1750–R1753 (1995).